23rd ABCM International Congress of Mechanical Engineering
December 6-11, 2015, Rio de Janeiro, RJ, Brazil

A ROUGHNESS SURFACE MODEL TO SIMULATE THE DRAG CRISIS USING A LAGRANGIAN VORTEX METHOD

Alex Mendonça Bimbato
Department of Energy, São Paulo State University (UNESP), Guaratinguetá, Brazil
alexbimbato@feg.unesp.br

Luiz Antonio Alcântara Pereira
Mechanical Engineering Institute, Federal University of Itajubá (UNIFEI), Itajubá, Brazil
luizantp@unifei.edu.br

Miguel Hiroo Hirata
State University of Rio de Janeiro (FAT-UERJ), Resende, Brazil
miguelhhirata@gmail.com

Abstract. *The purpose of this work is to present a roughness surface model to be used with the mesh free vortex method to simulate numerically the flow past a circular cylinder. The roughness model is based on the physics sense that roughness surfaces may stimulate turbulent boundary layer flows. The second-order velocity structure function of the filtered field is used to take into account the sub-grid scale phenomena. The results obtained in this work show that the roughness model developed is able to stimulate turbulent boundary layer flows and to capture the drag crisis.*

Keywords: *roughness model; sub-scale model; drag crisis; vortex method; panel method*

1. INTRODUCTION

The flow around bluff bodies can cause important physical phenomena, such as separation, vortex shedding and transition to turbulence. The transition to turbulence at a bluff body is one of the most studied phenomena by the scientific community. The parameter that governs the transition to turbulence is the Reynolds number, Re ($Re = U^* d^* / \upsilon$, where U^* is the incident flow velocity, d^* is the characteristic length and υ is the kinematic viscosity). The transition to turbulence begins at the bluff body wake and, as the Reynolds number increases, it reaches the shear layers, and for higher Reynolds numbers, it reaches the boundary layers.

Nishino (2007) classified the flow around a smooth and isolated circular cylinder in three regimes: subcritical ($Re < 2.0\times10^5 - 5.0\times10^5$), critical ($Re \cong 2.0\times10^5 - 5.0\times10^5$) and supercritical ($Re > 2.0\times10^5 - 5.0\times10^5$); Roshko (1961) included a fourth regime called transcritical ($Re > 3.5\times10^6$).

A particular interest surges when the transition to turbulence reaches the boundary layers. When this occurs the flow has more momentum to support the adverse pressure gradient and the separation points move to downstream causing the drag crisis. As the transition to turbulence at the boundary layers occurs at high Reynolds number flows, small perturbations can be amplified and, as consequence, can modify the aerodynamic behaviour of the bluff body. One of the most common perturbations found in engineering applications is the body surface roughness, which can anticipate the transition to turbulence. In order to reduce the flow complexity this paper studies the influence of the circular cylinder roughness surface in a high Reynolds number flow. Although the circular cylinders consist in simple bluff body geometry, many interesting flow characteristics can be studied with this simple shape.

The main difficulty to study turbulent flows around rough surfaces is related to the surface roughness characteristics. The surface roughness can be determined by the following parameters: (i) the relative roughness, ε^*/d^*, where ε^* is the surface protuberance's height and d^* is the circular cylinder diameter; (ii) the surface texture, what indicates how the protuberances are arranged on the surface.

One of the first works that studied the drag coefficient behaviour for a rough circular cylinder was done by Fage and Warsap (1929); they measured the mean drag coefficient, $\overline{C}_D$, and showed that, as the relative roughness (ε^*/d^*) increased, the drag crisis occurred at lower Reynolds number flows. Zdravkovich (2003) presents more details about the work done by Fage and Warsap (1929).

Guven *et al*. (1980) showed in a $\overline{C}_D \times Re$ diagram their results with the results obtained by Fage and Warsap (1929), Achenbach (1971) and Szechenyi (1975). The results present differences up to 60% for a given Reynolds number. These differences were attributed to some influencing factors, such as: aspect ratio, blockage ratio, turbulence level and the surface texture. The greater differences were observed in the supercritical flow regime which indicates the importance of the surface roughness. It is known that, in the supercritical flow, the viscous sublayer is too reduced that surface's protuberances cause disturbances in the boundary layer flow.

It can be noted in the literature a lack of numerical simulations at high Reynolds number flows ($Re \geq 1.0 \times 10^5$). An exception is the work done by Kawamura *et al*. (1986); the authors studied numerically the two-dimensional flow around a rough circular cylinder ($\varepsilon^*/d^* = 0.005$) at $10^3 < Re < 10^5$ using the finite difference method. Kawamura *et al*. (1986) obtained good results for $\overline{C}_D \times Re$ diagram. However, as they had instability problems with the finite difference method, the obtained $\overline{C}_D \times Re$ diagram did not even reach $Re = 1.0 \times 10^5$. No turbulence model was used by authors.

In the present work a two-dimensional roughness model is developed to be incorporated to a Lagrangian Vortex Method. The roughness model is associated to the second-order velocity structure function of the filtered field (Alcântara Pereira *et al*., 2002; Bimbato *et al*., 2012). The Lagrangian Vortex Method is used since it has been developed and applied for the analysis of complex, unsteady and vortical flows (Kamemoto, 2004). The most important features of the Discrete Vortex Method are: (i) it is a mesh free technique; (ii) it is a suitable technique for large eddy simulation; (iii) the computational efforts are directed only to the regions with non-zero vorticity and not to all fluid domain as is done in the eulerian description; (iv) the far away boundary condition is taken into account automatically.

2. GOVERNING EQUATIONS

Figure 1 shows the two-dimensional, incompressible and unsteady viscous flow around an isolated circular cylinder, where U^* is the mainstream velocity, Ω is the fluid domain defined by surface $S = S_1 \cup S_2$, being S_1 the body surface and S_2 the far away boundary. The flow depicted in Fig. 1 is governed by the continuity and the Navier-Stokes Equations, which can be written in the form (Alcântara Pereira *et al*., 2002):

$$\frac{\partial \overline{u}_i}{\partial x_i} = 0 \tag{1}$$

$$\frac{\partial \overline{u}_i}{\partial t} + \frac{\partial}{\partial x_j}\left(\overline{u}_i \overline{u}_j\right) = -\frac{1}{\rho}\frac{\partial \overline{p}}{\partial x_i} + 2\frac{\partial}{\partial x_j}\left[\left(\upsilon + \upsilon_t\right)\overline{S}_{ij}\right] \tag{2}$$

where $\overline{u}_i$ is the velocity filtered field ($u_i = \overline{u}_i + u_i'$; u_i' is the velocity fluctuation), $\overline{p}$ is the pressure filtered field, υ_t is the eddy viscosity and $\overline{S}_{ij}$ is the deformation tensor of the filtered field (Smagorinsky, 1963).

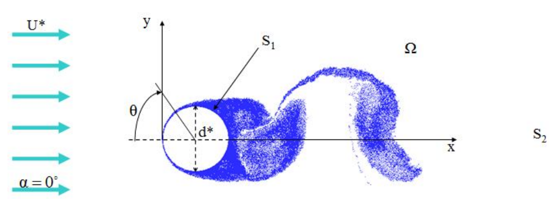

Figure 1. Flow around an isolated circular cylinder

Considering that the small scales are homogeneous and isotropic and using a relation proposed by Batchelor (1953), Lesieur and Métais (1996) proposed to use the local kinetic energy spectrum in order to calculate the eddy viscosity:

$$\upsilon_t\left(\boldsymbol{x}, \Delta^+, t\right) = 0.105 C_k^{-3/2} \Delta^+ \sqrt{\overline{F}_2\left(\boldsymbol{x}, \Delta^+, t\right)} \tag{3}$$

where $C_k = 1.4$ is the kolmogorov constant and $\overline{F}_2\left(\boldsymbol{x}, \Delta^+, t\right)$ is the local second-order velocity structure function of the filtered field, defined as:

$$\overline{F}_2\left(\boldsymbol{x}, \Delta^+, t\right) = \left\| \overline{\boldsymbol{u}}\left(\boldsymbol{x}, t\right) - \overline{\boldsymbol{u}}\left(\boldsymbol{x} + \boldsymbol{r}, t\right) \right\|^2_{|\boldsymbol{r}| = \Delta^+} \tag{4}$$

where $\overline{\overline{\boldsymbol{u}}(\boldsymbol{x},t)-\overline{\boldsymbol{u}}(\boldsymbol{x}+\boldsymbol{r},t)}$ is the average speed differences between the center of a sphere located at $\boldsymbol{x}$ with radius $|\boldsymbol{r}| = \Delta^+$ and points located on the sphere surface. In this formulation the center of the sphere is defined as a point of the flow field where one wants to calculate the turbulent activity. The above equation is used in three-dimensional flows; since the present work deals with a two-dimensional flow the second-order velocity structure function model needs to be adapted to two-dimensional problems (see Section 3.3).

Therefore Eq. (1) and Eq. (2) are used to simulate the large eddy phenomena with the Discrete Vortex Method and the small eddy ones are taken into account by eddy viscosity (Eq. (3)) which is modeled by local second-order velocity structure function of the filtered field (Eq. (4)).

The impermeability condition, Eq. (5), demands that the normal velocity component of the fluid particle, $\overline{u}_n$, should be equal to the normal velocity components of the surface S_1, v_n. The no-slip condition, Eq. (6), demands that the tangential velocity component of the fluid particle, $\overline{u}_\tau$, should be equal to the tangential velocity component of the surface S_1, v_τ. The far away boundary condition is given by Eq. (7). The equations are respectively:

$$\overline{u}_n - v_n = 0 \text{, on } S_1 \tag{5}$$

$$\overline{u}_\tau - v_\tau = 0 \text{, on } S_1 \tag{6}$$

$$|\overline{\boldsymbol{u}}| \to U^* \text{, on } S_2 \tag{7}$$

In order to make all the quantities in the equations above non-dimensional, U^* and d^* are used. The non-dimensional time is given by $t^* U^* / d^*$. In the formulation above the symbol * means dimensional quantities.

3. NUMERICAL SOLUTION

The essence of the Lagrangian Vortex Method is to discretize the vorticity field using Lamb discrete vortices in a manner that (Kundu, 1990):

$$\overline{\boldsymbol{\omega}}(\boldsymbol{x},t) = \sum_{k=1}^{NV} \frac{\Gamma_k}{\pi \sigma_{0_k}^2} exp\left(-\frac{|\boldsymbol{x}|^2}{\sigma_{0_k}^2} \right) \tag{8}$$

where $\overline{\boldsymbol{\omega}}$ ($\overline{\boldsymbol{\omega}} = \nabla \times \overline{\boldsymbol{u}}$) is the vorticity filtered field, NV is the total number of discrete vortices in the fluid domain, Γ_k is the strength of the discrete vortex k necessary to satisfy Eq. (6) and σ_0 is the Lamb vortex core given by (Mustto *et al.*, 1998; Bimbato, 2012):

$$\sigma_0 = 4.48364 \sqrt{\frac{\Delta t}{Re}} \chi \tag{9}$$

The time step Δt is calculated from an estimate of the convective length and velocity scales of the flow. χ is a factor obtained through numerical experiences in order to determine the appropriate value of the Lamb vortex core, considering the influence of the method used to represent the solid boundaries; more details can be found in Bimbato (2012).

In this work the circular cylinder surface is represented by source flat panels (Katz and Plotkin, 1991). Each panel has a pivotal point where Eqs. (5) and (6) must be imposed. The sources strength distributed along the flat panels satisfy Eq. (5). A Lamb discrete vortex is positioned at a shedding point defined near each flat panel to satisfy Eq. (6). Figure 2(a) shows one of the source flat panels used to represent the circular cylinder surface; it illustrates how the vorticity is generated on a smooth surface by the Vortex Method (co is the pivotal point, $pshed'$ is the shedding point, eps' is the distance between the pivotal point and the center of the Lamb discrete vortex and σ_0 is the Lamb vortex core).

The problem is solved by taking the curl of Eq. (2) and considering Eq. (1) to obtain the vorticity equation. For a 2-D flow this equation is scalar (the pressure term is absent), and it can be written as:

$$\frac{\partial \overline{\omega}}{\partial t} + (\overline{\boldsymbol{u}} \cdot \nabla)\overline{\omega} = \frac{1}{Re_c} \nabla^2 \overline{\omega} \tag{10}$$

where $Re_c = U^* d^* / \upsilon + \upsilon_t$ is the Reynolds number modified by eddy viscosity.

(a) smooth surface (b) rough surface

Figure 2. Vorticity generation process on the Discrete Vortex Method

Depending on the Reynolds number flow, a roughness surface can stimulate the development of turbulence in the flow. The roughness model developed in this work is based on this physical sense. Thus, the second-order velocity structure function of the filtered field (Eq. (4)) is used with some adaptations in order to obtain the turbulent activity around the shedding point of each panel.

In order to determine the turbulent activity around the shedding point of an i panel ($pshed_i'$ point shown in Fig. 2(b)), a semicircle centered on shedding point i with radius $\|\boldsymbol{b}\| = 2\varepsilon - eps'$ is defined ($\varepsilon = \varepsilon^* / d^*$). A point set, called rough points, are defined on the semicircle. The average speed differences necessary to determine the second-order velocity structure function of the filtered field (see Eq. (4)) is computed between the center of the semicircle ($pshed_i'$ point) and the rough points. Thus:

$$\overline{F}_{2_i}(t) = \frac{1}{NR} \sum_{w=1}^{NR} \left\| \overline{\boldsymbol{u}}_{t_i}(\boldsymbol{x}_i, t) - \overline{\boldsymbol{u}}_{t_w}(\boldsymbol{x}_i + \boldsymbol{b}, t) \right\|_w^2 (1 + \varepsilon) \tag{11}$$

where $\boldsymbol{u}_t$ is the velocity on the points, NR is the number of rough points and $(1+\varepsilon)$ represents the kinetic energy gain due to the roughness effects. The authors used 21 rough points on each semicircle defined around each shedding point; this number is enough to obtain a reasonable value for the average speed differences.

The eddy viscosity associated to the shedding point of panel i, taking into account the roughness effects is given by (compare with Eq. (3)):

$$\upsilon_{t_i}(t) = 0.105 C_k^{-3/2} \sigma_{0_k} \sqrt{\overline{F}_{2_i}(t)} \tag{12}$$

where σ_{0_k} is the vortex core of the k discrete vortex positioned at i shedding point (see Fig. 2(b)).

As consequence, the Reynolds number needs to be modified:

$$Re_{c_i}(t) = \frac{U^* d^*}{\upsilon + \upsilon_{t_i}(t)} \tag{13}$$

It is important to say that the Reynolds number modification occurs locally, just on the discrete vortices shedding point, and when the roughness effects are important ($\upsilon_{t_i}(t) \neq 0$).

Equation (9) shows the relation between the Lamb vortex core and the Reynolds number. If the roughness effects are important ($\upsilon_{t_i}(t) \neq 0$), the Lamb vortex core must be modified. Thus:

$$\sigma_{0c_k}(t) = 4.48364 \sqrt{\frac{\Delta t}{Re} \left(1 + \frac{\upsilon_{t_i}(t)}{\upsilon} \right)} \chi \tag{14}$$

where σ_{0c_k} is the vortex core of the k discrete vortex positioned at i shedding point, modified by roughness model. As consequence, depending on the roughness effects, the discrete vortex shedding position can be modified during all the time of the numerical simulation. It is important to emphasize that there is no change on the body surface. The roughness surface effects are taken into account by an inertial effect imposed on the discrete vortices generation process. The roughness model developed here is based only on the physics of turbulent flows.

3.1 The Viscous Splitting Algorithm

The governing equation in 2-D Vortex Methods is the vorticity transport equation shown in Eq. (10). Chorin (1973) proposed an algorithm that splits convective-diffusive operator of Eq. (10) in the form:

$$\frac{D\overline{\omega}}{Dt} = \frac{\partial \overline{\omega}}{\partial t} + (\overline{\boldsymbol{u}} \cdot \nabla)\overline{\omega} = 0 \tag{15}$$

$$\frac{\partial \overline{\omega}}{\partial t} = \frac{1}{Re_c} \nabla^2 \overline{\omega} \tag{16}$$

According to the Lagrangian form of Eq. (15), the convective process is solved using a first order Euler scheme, after to compute the velocity vector field at each discrete vortex k present in the fluid domain. The velocity vector field is composed by three contributions: (i) the mainstream speed, $\overline{ui}(\boldsymbol{x},t)$, Eq. (17); (ii) the solid boundaries (Panel's Method, Katz and Plotkin, 1991), $\overline{ub}(\boldsymbol{x},t)$, Eq. (18); (iii) the vortex-vortex interaction (the Biot-Savart Law), $\overline{uv}(\boldsymbol{x},t)$, Eq. (19). Thus:

$$\overline{ui_1} = 1 \qquad \text{and} \qquad \overline{ui_2} = 0 \tag{17}$$

$$\overline{ub_k^n}(\boldsymbol{x}_k, t) = \sum_{p=1}^{NP} \sigma_p c_{kp}^n \left[\boldsymbol{x}_k(t) - \boldsymbol{x}_p\right], \qquad n = 1,2 \qquad \text{and} \qquad k = 1, NV \tag{18}$$

$$\overline{uv_k^n}(\boldsymbol{x}_k, t) = \sum_{j=1}^{NV} \Gamma_j c_{kj}^n \left[\boldsymbol{x}_k(t) - \boldsymbol{x}_j(t)\right], \qquad n = 1,2 \qquad \text{and} \qquad k = 1, NV \tag{19}$$

where NV is the total number of discrete vortices present in the flow at instant t, NP is the total number of source flat panels, $\sigma_p = constant$ is the source density per unit length, $c_{kp}^n\left[\boldsymbol{x}_k(t) - \boldsymbol{x}_p\right]$ is the $n-th$ component of the velocity induced at discrete vortex k by p panel, Γ_j is the intensity of the j vortex and $c_{kj}^n\left[\boldsymbol{x}_k(t) - \boldsymbol{x}_j(t)\right]$ is the $n-th$ component of the induced velocity at a discrete vortex k by a discrete vortex j. Note that the intensity Γ_j of each discrete vortices are determined using the no-slip condition and the source strengths are determined using the impermeability condition. These equations are satisfied simultaneously during each time step of the simulation.

In this paper, the viscous diffusion (Eq. (16)) is simulated using a fractional random walk method introduced by Chorin (1973):

$$\varsigma_k(t) = \sqrt{\frac{4\,\Delta t}{Re_c} ln\left(\frac{1}{P}\right)} \left[cos(2\pi Q) + sin(2\pi Q)\right] \tag{20}$$

where P and Q are random numbers, being $0 < P < 1$ and $0 < Q < 1$.

3.2 The Turbulence Model

Equation (20) shows that turbulence effects must be considered in diffusion process. Thus, in this stage there is a connection between the larger scales and the smaller ones, which is made by eddy viscosity (Eq. (3)). As described in Section 2, the local turbulent activities are determined by the second-order velocity structure function of the filtered field (Eq. (4)), which must be adapted to the two-dimensional problem, according to (Alcântara Pereira *et al.*, 2002): **(i)** the points where velocities must be calculated are placed inside a circular crown centered at a reference vortex j, defined by $r_{int} = 0.1\sigma_{0_j}$ and $r_{ext} = 4.0\sigma_{0_j}$, where r_{int} and r_{ext} are the internal and external radius of the circular crown, respectively, and σ_{0_j} is the core of the Lamb discrete vortex under analysis. A statistical analysis was done by Bimbato *et al.* (2012) to determine r_{int} and r_{ext}; **(ii)** to compute the second-order velocity structure function of the filtered field, the points where velocities are calculated are the same as the positions of the vortices, which are near the vortex under analysis (inside the circular crown). Thus:

$$\overline{F}_{2_j} = \frac{1}{N}\sum_{k=1}^{N}\left\|\overline{\boldsymbol{u}}_{t_j}\left(\boldsymbol{x}_j\right)-\overline{\boldsymbol{u}}_{t_k}\left(\boldsymbol{x}_j+\boldsymbol{r}_k\right)\right\|_k^2\left(\frac{\sigma_{0_j}}{\boldsymbol{r}_k}\right)^{2/3} \tag{21}$$

where $\overline{\boldsymbol{u}}_t$ is the total velocity in the point ($\overline{u}_t = \overline{ui} + \overline{ub} + \overline{uv}$), N indicates the number of discrete vortices inside the circular crown and $\boldsymbol{r}_k$ is the distance between the discrete vortex under analysis ($j-th$ discrete vortex) and the discrete vortices inside the circular crown (each $k-th$ discrete vortex).

3.3 Aerodynamic Loads

With the vorticity field it is possible to obtain a Poisson equation for the pressure and its solution is obtained through the following integral formulation (Shintani and Akamatsu, 1994):

$$H\overline{Y}_p - \int_{S_1}\overline{Y}\nabla\Xi_p\cdot\boldsymbol{e}_n dS = \iint_{\Omega}\nabla\Xi_p\cdot(\overline{\boldsymbol{u}}\times\overline{\boldsymbol{\omega}})d\Omega - \frac{1}{Re}\int_{S_1}\left(\nabla\Xi_p\times\overline{\boldsymbol{\omega}}\right)\cdot\boldsymbol{e}_n dS \tag{22}$$

where the pressure is computed at $p-th$ pivotal point, co (see Fig. 2), $H = 1.0$ in the fluid domain, $H = 1/2$ on the boundaries, Ξ is a fundamental solution of Laplace Equation, $\overline{Y}$ is the specific work and $\boldsymbol{e}_n$ is the unit vector normal to each source flat panel. The drag and lift forces are obtained by pressure integration.

4. SIMULATION OF FLOWS AROUND A SMOOTH OR A ROUGH CIRCULAR CYLINDER

The aim of this section is to show that the roughness model can develop turbulent boundary layer flows from subcritical Reynolds number flow of $Re = 1.0\times10^5$. The following numerical parameters used in this work were validated by Bimbato *et al*. (2013): number of source flat panels used to represent the cylinder surface ($NP = 300$), time increment ($\Delta t = 0.05$) and the Lamb vortex core ($\sigma_0 = 0.001$).

Table 1 shows the aerodynamic characteristics of the flow around a smooth cylinder as compare to the ones of the flow around a rough cylinder. It is included the experimental result obtained by Blevins (1984) for a smooth cylinder.

Table 1. Mean drag coefficient ($\overline{C}_D$) and separation point (θ_{sep}) for the circular cylinder.

$\mathbf{Re = 1.0\times10^5}$	$\boldsymbol{\varepsilon}$	$\overline{\mathbf{C}}_{\mathbf{D}}$	$\boldsymbol{\theta}_{\mathbf{sep}}$
Blevins (1984) - experimental	0.0000	1.20	82°
Present Simulation	0.0000	1.22	77°
Present Simulation	0.0010	1.19	80°
Present Simulation	0.0020	1.13	85°
Present Simulation	0.0045	1.02	101°
Present Simulation	0.0070	1.07	87°

The aerodynamic loads computations are evaluated between $37.50 \le t \le 75.00$ and as can be seen, they agree quite well with the experimental result for the smooth cylinder; the differences in the drag force is less than 2.0 %.

It can be seen from Table 1 and Fig. 3 that the smaller roughness tested ($\varepsilon = 0.001$) causes just a small perturbation in the boundary layer flow. There is no significant change on body's aerodynamic behaviour. However, increasing the roughness surface ($\varepsilon = 0.002$) one can note the beginning of the drag crisis, but the flow regime is still subcritical. See how the vortex shedding mechanism is almost the same in Fig. 3a and Fig. 3b.

On the other hand when the roughness model simulates a surface with relative roughness of $\varepsilon = 0.007$ the flow regime is not subcritical anymore.

In this situation, the boundary layer flow separates at $\theta \cong 87^\circ$; the separation points move downstream (for the smooth cylinder the separation takes place at $\theta \cong 77^\circ$). As a consequence, the drag coefficient is reduced approximately by 12.4 % (see Table 1).

Computed values for drag coefficient are plotted in Fig. 3d. One can observe weaker periodic oscillations as compared to the ones of Fig. 3a.

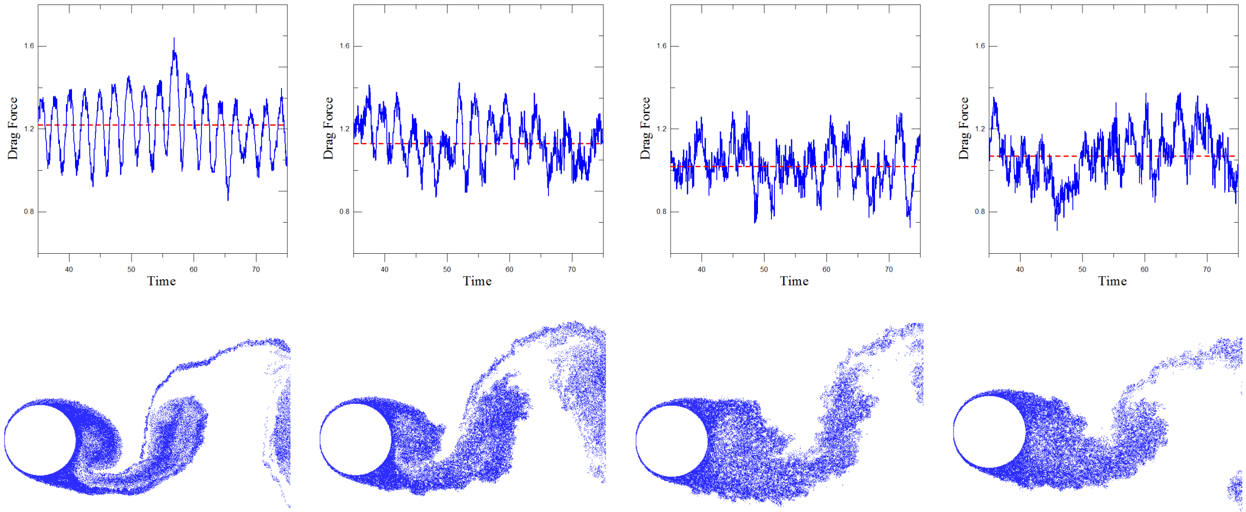

(a) $\varepsilon = 0.0000$ (b) $\varepsilon = 0.0020$ (c) $\varepsilon = 0.0045$ (d) $\varepsilon = 0.0070$

Figure 3. Temporal series for the drag force and near wake structures for the flow past a circular cyinder ($Re = 1.0 \times 10^5$).

The changes in flow behaviour were expected since the roughness tested ($\varepsilon = 0.007$) is able to cause supercritical flows (Fage and Warsap, 1929; Zdravkovich, 2003). Due to the delay of the boundary layer separation (from $\theta \cong 77^\circ$ to $\theta \cong 87^\circ$) and to the reduction of the drag coefficient (from $\overline{C}_D = 1.22$ to $\overline{C}_D = 1.07$), it can be said that the roughness model developed in this work captured well the drag crisis.

An evidence that shows the flow regime is now supercritical can be seen observing Table 1 and Fig. 4. As the roughness surface increases the mean drag force decreases and after reaches a minimum value (that is not necessarily when $\varepsilon = 0.0045$), the mean drag force increases again (Table 1). Figure 4 shows that this behaviour is typical of supercritical flow regimes.

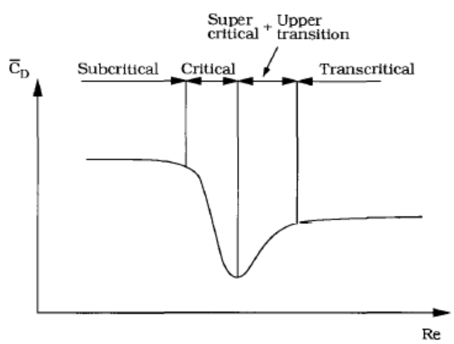

Figure 4. General form of a $\overline{C}_D \times Re$ diagram for the flow past a circular cylinder (Sumer and Fredsøe, 2006).

Observing Fig. 3 it is possible to see how the roughness model affects the vortex shedding mechanism (compare Fig. 3a and Fig. 3b with Fig. 3c and Fig. 3d). The near wake development is modified by the inertial effect imposed by the roughness model what causes the drag crisis.

5. CONCLUSIONS

In this work the authors developed a roughness surface model able to capture the drag crisis in the flow past a circular cylinder. The numerical model developed is based on the physical sense that roughness surfaces may stimulate turbulent boundary layer flows which are the responsible for the drag crisis. The model affects only the boundary layer; the body surface remains unchanged.

The comparison between the numerical results obtained with the roughness model and experimental results were avoided since it is too difficult to reproduce exactly the same roughness parameters (roughness elements height and roughness surface texture). Even the experimental results present differences in the mean drag coefficient measured of about 60 % for the same supercritical Reynolds number flow as confirmed by Guven *et al*. (1980). Thus, it is not fair to compare results in this range of Reynolds number flows.

In a near future the authors will test the roughness model developed in this work to simulate turbulent boundary layer flows on slender bodies.

6. ACKNOWLEDGEMENTS

This study was supported by Brazilian Research Agency (CNPq), Proc. 142804/2008-8.

7. REFERENCES

Achenbach, E., 1971. "Influence of Surface Roughness on the Cross-Flow around a Circular Cylinder". *Journal of Fluid Mechanics*, Vol. 46, pp. 321-335.

Alcântara Pereira, L. A., Ricci, J. E. R., Hirata, M. H. and Silveira Neto, A., 2002. "Simulation of the Vortex-Shedding Flow about a Circular Cylinder with Turbulence Modeling". *CFD Journal*, Vol. 11, n. 3, pp. 315-322, October.

Batchelor, G. K., 1953. *The Theory of Homogeneous Turbulence*. Cambridge Univ. Press, Cambridge, England, UK.

Bimbato, A. M., 2012. *Study of Turbulent Flows around a Smooth or a Rough Bluff Body Using the Discrete Vortex Method*, D.Sc. Thesis, Institute of Mechanical Engineering, UNIFEI, Itajubá, MG, Brazil (in Portuguese).

Bimbato, A. M., Alcântara Pereira, L. A. and Hirata, M. H., 2012. "Corrected Lagrangian LES Model for Vortex Method". *8th Spring School on Transition and Turbulence*, São Paulo, Sep. 24-28.

Bimbato, A. M., Alcântara Pereira, L. A. and Hirata, M. H., 2013. "Suppression of vortex shedding on a bluff body". Journal of Wind Engineering and Industrial Aerodynamics, Vol. 121, pp. 16-28.

Blevins, R. D., 1984. *Applied Fluid Dynamics Handbook*. Van Nostrand Reinhold Co.

Chorin, A. J., 1973. "Numerical Study of Slightly Viscous Flow". *Journal of Fluid Mechanics*, Vol. 57, pp. 785-796.

Fage, A. and Warsap, J. H., 1929. "The Effects of Turbulence and Surface Roughness on the Drag of a Circular Cylinder". *Brit. Aeronautical Research Council*, Rep and Memo 1283.

Guven, O., Farell, C. and Patel, V. C., 1980. "Surface Roughness Effects on the Mean Flow Past Circular Cylinders". *Journal of Fluid Mechanics*, Vol. 98, pp. 673-701.

Kamemoto, K., 2004. "On Contribution of Advanced Vortex Element Methods toward Virtual Reality of Unsteady Vortical Flows in the New Generation of CFD". *J. Braz. Soc. Mech. Sci. & Eng.*, Vol. 26, n. 4, Rio de Janeiro, Oct. / Dec..

Katz, J. and Plotkin, A., 1991. *Low Speed Aerodynamics: From Wing Theory to Panel Methods*. McGraw Hill, Inc.

Kawamura, T., Takami, H. and Kuwahara, K., 1986. "Computation of High Reynolds Number Flow around a Circular Cylinder with Surface Roughness". *Fluid Dynamics Research*, Vol. 1, pp. 145-162.

Kundu, P. K., 1990. *Fluid Mechanics*, Academic Press.

Lesieur, M. and Métais, O., 1996. "New Trends in Large Eddy Simulation of Turbulence". *A Review in Fluid Mechanics*, Vol. 28, pp. 45-82.

Mustto, A. A., Hirata, M. H. and Bodstein, G. C. R., 1998. "Discrete Vortex Method Simulation of the Flow around a Circular Cylinder with and without Rotation". A.I.A.A. Paper 98-2409, *Proceedings of the 16th A.I.A.A. Applied Aerodynamics Conference*, Albuquerque, NM, USA, June.

Nishino, T., 2007. *Dynamics and Stability of Flow past a Circular Cylinder in Ground Effect*. Ph.D. Thesis, Faculty of Engineering Science and Mathematics, University of Southampton.

Roshko, A., 1961. "Experiments on the Flow past a Circular Cylinder at Very High Reynolds Number". *Journal of Fluid Mechanics*, Vol. 10, pp. 345-356.

Shintani, M., Akamatsu, T., 1994. Investigation of Two-Dimensional Discrete Vortex Method with Viscous Diffusion Model. CFD Journal, vol. 3, n. 2, pp. 237-254.

Smagorinsky, J., 1963. "General Circulation Experiments with the Primitive Equations". *Mon. Weather Rev.*, Vol. 91, n. 3, pp. 99-164.

Sumer, B. M. and Fredsøe, J., 2006. "Hidrodynamics around Cylindrical Structures". *Advanced Series on Ocean Engineering*, Vol. 26, 550p.

Szechenyi, E., 1975. "Supercritical Reynolds Number Simulation for Two Dimensional Flow over Circular Cylinders". *Journal of Fluid Mechanics*, Vol. 70, pp. 529-542.

Zdravkovich, M. M., 2003. *Flow around Circular Cylinders. Vol. 2: Applications*. Oxford University Press, Oxford, U.K.

8. RESPONSIBILITY NOTICE

The authors are the only responsible for the printed material included in this paper.